

This document is the accepted manuscript version of the following article:
Chen, G., Hofstetter, T. B., & Gorski, C. A. (2020). Role of carbonate in thermodynamic relationships describing pollutant reduction kinetics by iron oxide-bound Fe²⁺. *Environmental Science and Technology*, 54(16), 10109-10117. <https://doi.org/10.1021/acs.est.0c02959>

The role of carbonate in thermodynamic relationships describing pollutant reduction kinetics by iron oxide-bound Fe²⁺

Gongde Chen,¹ Thomas B. Hofstetter,^{2,3} and Christopher A. Gorski^{1,*}

¹ Department of Civil & Environmental Engineering, Pennsylvania State University, University Park, Pennsylvania, United States

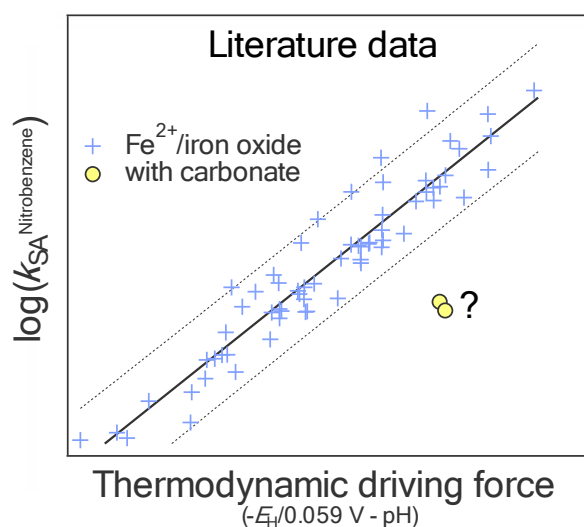
² Eawag, Swiss Federal Institute of Aquatic Science and Technology, Dübendorf, Switzerland

³ Institute of Biogeochemistry and Pollutant Dynamics (IBP), Swiss Federal Institute of Technology, ETH Zürich, Zürich, Switzerland

* Corresponding author, e-mail: gorski@psu.edu, phone (814) 865-5673, fax (814) 863-7304

1 ABSTRACT

2 The reduction of environmental pollutants by Fe^{2+} bound to iron oxides is an important process that
3 determines pollutant toxicities and mobilities. Recently, we showed that pollutant reduction rates
4 depend on the thermodynamic driving force of the reaction in a linear free energy relationship that
5 was a function of the solution pH value and the reduction potential, E_{H} , of the interfacial $\text{Fe}^{3+}/\text{Fe}^{2+}$
6 redox couple. In this work, we studied how carbonate affected the free energy relationship by
7 examining the effect that carbonate has on nitrobenzene reduction rates by Fe^{2+} bound to goethite
8 ($\alpha\text{-FeOOH}$). Carbonate slowed nitrobenzene reduction rates by inducing goethite particle
9 aggregation, as evidenced by surface charge and particle size measurements. We observed no
10 evidence for carbonate affecting $\text{Fe}^{3+}/\text{Fe}^{2+}$ reduction potentials or the mechanism of nitrobenzene
11 reduction. The linear free energy relationship accurately described the data collected in the presence
12 of carbonate when we accounted for the effect it had on the reactive surface area of goethite. The
13 findings from this work provide a framework for determining why common groundwater
14 constituents affect the E_{H} -dependence of reaction rates involving oxide-bound Fe^{2+} as a reductant.



15 INTRODUCTION

16 Ferrous iron (Fe^{2+}) can reduce and simultaneously alter the toxicities and/or solubilities of several
17 classes of environmental pollutants found in groundwater.¹⁻¹² Consequently, Fe^{2+} is a critical
18 reductant to account for in naturally attenuated and engineered remediation systems.¹³⁻¹⁸ Prior work
19 has established that aqueous Fe^{2+} in the presence of an iron (oxyhydr)oxide (i.e., an “iron oxide”)
20 reduces pollutants far more quickly than aqueous Fe^{2+} alone,^{2, 9, 14, 19-27} with reduction rates
21 depending on the redox properties of the iron oxide present.^{2, 4-9, 14, 16, 21, 28-41} This effect is a result
22 of the iron oxide influencing what Fe^{3+} oxidation product forms.^{28, 30, 42, 43} When aqueous Fe^{2+}
23 oxidizes in the absence of an iron oxide, it tends to form an aqueous Fe^{3+} complex or ferrihydrite.⁴⁴
24 When Fe^{2+} oxidizes in the presence of a crystalline iron oxide, however, it tends to form a more
25 thermodynamically stable iron oxide phase, typically via homoepitaxial growth.^{32, 45, 46} Thus the
26 presence of an iron oxide alters the reduction potential (E_{H}) value of the $\text{Fe}^{3+}/\text{Fe}^{2+}$ redox couple by
27 changing the Fe^{3+} speciation (i.e., the iron oxide that forms).

28 Recently, we demonstrated that measured E_{H} values for solutions containing iron oxides and
29 aqueous Fe^{2+} were fully consistent with those calculated from reference thermodynamic values for
30 the Fe^{2+} oxidation and mineral growth process, indicating that thermodynamic calculations can be
31 used to accurately estimate E_{H} values for suspensions containing iron oxides and aqueous Fe^{2+} .³⁰
32 We then showed that the rate constant at which oxide-bound Fe^{2+} reduced organic compounds
33 depended on the thermodynamic driving for Fe^{2+} oxidation, as represented by E_{H} values of
34 suspensions.²⁸ Calculated E_{H} values could be used to construct a linear free energy relationship that
35 correlated reduction rate constants of nitroaromatic compounds by oxide-bound Fe^{2+} , expressed as
36 logarithms of the surface-area-normalized reaction rate constants, $\log(k_{\text{SA}})$, to the thermodynamic
37 driving force of the reaction (**Section S1, Figure S1A, Table S1**):²⁸

38
$$\log(k_{SA}) = a \cdot \frac{E_H}{0.059 \text{ V}} + b \cdot \text{pH} + c \quad (1)$$

39 where the E_H term is the reduction potential for the half-reaction of Fe^{2+} oxidation to an iron oxide
40 (shown here for goethite):



42 The pH term in eq. 1 accounts for the proton transfer step(s) to nitrobenzene at or before the rate-
43 determining step of the reduction reaction. Coefficient c is the y-intercept.²⁸ The coefficients a and
44 b in eq. 1 were both found to be -1 in our prior work,²⁸ which included data from six independent
45 studies using goethite, hematite, lepidocrocite, ferrihydrite, and/or magnetite.^{9, 14, 21, 28, 36, 47} The
46 numerical values of these coefficients stand for the consensus reaction mechanism in which proton
47 and electron transfers contribute to the rate-limiting step of oxide-bound Fe^{2+} oxidation by
48 nitroaromatic compounds.^{28, 48-50} Our observation that data for different iron oxides could be fit with
49 a single c -term suggested that surface-area normalization of observed rate constants was an adequate
50 procedure to account for reactive oxide-bound Fe^{2+} sites that interact with nitroaromatic compounds.

51 In the aforementioned studies, the solutions only contained iron oxide particles, aqueous
52 Fe^{2+} , an organic pH buffer, and often a background electrolyte. Interestingly, experiments conducted
53 with additional species commonly found in groundwater (i.e., carbonate, humic acid, or a model
54 humic acid) yielded data that deviate from the free energy relationship in that reaction rate constants
55 were higher and lower than predicted by the calculated E_H of the free energy relationship (eq. 1,
56 **Figure S1B**).^{39, 51-53} Understanding why these species cause data to diverge from the free energy
57 relationship is an essential step that must be addressed to use the relationship to describe the
58 reactivity of oxide-bound Fe^{2+} in natural and engineered environmental systems. The additional
59 species could alter the free energy relationship in two ways. First, they could change the slope of the

60 free energy relationship (i.e., the a and/or b terms in eq. 1), which represents the relationship
61 between the thermodynamic driving force of the reaction and the reaction rate.²⁸ This would occur
62 if the species change the reaction mechanism and/or the rate-limiting step of the reaction. Second,
63 the species could alter the y-intercept (i.e., the c term in eq. 1), which would occur if the species
64 change the number of reactive sites on the iron oxide surface, the frequency of interactions between
65 the electron acceptor and reactive oxide-bound Fe^{2+} sites, and/or the Fe^{2+} oxidation product that
66 forms (due to a change in the standard reduction potential, E_{H}^0 , for the $\text{Fe}^{3+}/\text{Fe}^{2+}$ half reaction).
67 Unfortunately, datasets such as those shown in **Figure S1B**, lack a sufficient amount of information
68 to conclusively discriminate among these possibilities.

69 The goal of this work was to determine why groundwater constituents can cause data to
70 deviate from the generalized linear free energy relationship describing organic compound reduction
71 rates with oxide-bound Fe^{2+} . Specifically, we investigated how and why the presence of carbonate
72 causes data to deviate during the reduction of nitrobenzene by Fe^{2+} bound to goethite. We used
73 nitrobenzene as the model contaminant because it does not sorb or react with iron oxides in the
74 absence of aqueous Fe^{2+} , meaning the nitrobenzene disappearance rate is equal to the reduction
75 rate.^{51, 54} We focused on carbonate as a model species and examined how it influenced Fe^{2+} uptake,
76 $\text{Fe}_{(\text{aq})}^{2+}/\text{goethite}$ E_{H} values, goethite aggregation, goethite surface charges, and nitrobenzene reduction
77 rate constants at different pH values. Because equilibrium constants are available to describe
78 complexation reactions between Fe^{2+} and carbonate,^{33, 55} the collected data allowed us to
79 discriminate among the above hypotheses. That is, we could examine how carbonate influenced the
80 free energy relationship between reaction rate constants and the thermodynamic driving force of the
81 reaction in terms of the slope and y-intercept. We conclude by using these data to offer a more

82 general approach for determining why other groundwater constituents, such as humic acids, alter
83 pollutant reduction rate constants.

84 **MATERIALS AND METHODS**

85 All chemicals were used as purchased, except cyanomethyl viologen, which was synthesized as
86 previously described.⁵⁶ All experiments were conducted at room temperature under anaerobic
87 conditions inside a glovebox (MBraun Unilab Workstation, 100% N₂ atmosphere, < 0.1 ppm O₂).
88 All aqueous solutions were prepared in deionized (DI) water (Millipore Milli-Q system, resistivity >
89 18 MΩ·cm) purged with N₂ (> 99.99%) for at least 3 h before being brought into the glovebox.

90 The pH buffer solutions contained 25 mM KCl and 25 mM pH buffer. The pH buffer used
91 at pH 6.0 and 6.5 was 2-N-morpholinoethanesulfonic acid (MES, p*K*_a 6.1, Aresco, ≥ 99%) and the
92 pH buffer used at pH 7.0 was 3-N-morpholinopropanesulfonic acid (MOPS, p*K*_a 7.2, EMD
93 Chemicals Inc., ≥ 99%). Carbonate stock solutions were freshly made inside the glovebox by
94 dissolving solid NaHCO₃ in deoxygenated DI water. The stock solutions were kept in sealed glass
95 vials with little headspace to avoid the loss of carbonate to the N₂ atmosphere. Ferrous chloride
96 (FeCl₂, Acros, anhydrous, 99%) was received in a sealed ampule and was transferred to the glovebox
97 to make a 0.2 M aqueous Fe²⁺ stock solution, which was acidified with a few drops of 5 M HCl to
98 avoid inadvertent oxidation. Cyanomethyl viologen was dissolved in deoxygenated DI water to make
99 a 10 mM mediator stock solution. Nitrobenzene (Reagent grade, Sigma-Aldrich) was transferred to
100 a small amber vial with little headspace and taken into the glovebox to make a 10 mM stock solution
101 in deoxygenated methanol.

102 ***Goethite Synthesis and Characterization***

103 Goethite was synthesized using an established method.⁵⁷ Briefly, 180 mL 5 M NaOH was added to
104 100 mL 0.1 M Fe(NO₃)₃ solution with vigorous stirring. The suspension was diluted to 2 L with DI
105 water and heated at 70°C for 60 h. The produced solid was washed with DI water by centrifugation,
106 freeze-dried, ground in a mortar, and sieved (200 mesh). The crystal phase of the synthesized
107 goethite was confirmed by X-ray diffraction (Malvern Panalytical Empyrean) with a Co irradiation
108 source ($K_{\alpha 1} = 1.7890 \text{ \AA}$, $K_{\alpha 2} = 1.7929 \text{ \AA}$) operated at 40 kV and 40 mA. All the diffraction peaks
109 (**Figure S2**) were consistent with goethite (PDF# 29-0713). The specific surface area of the goethite
110 (36 m²/g) was measured by N₂ sorption isotherms in liquid nitrogen (ASAP 2020 Automated Surface
111 Area and Porosimetry System) and calculated by the multi-point Brunauer-Emmett-Teller (BET)
112 method.⁵⁸

113 ***Fe²⁺ Uptake and Mediated Potentiometric Measurements***

114 Fe²⁺ uptake experiments were conducted inside the glovebox by measuring the difference between
115 initial and final aqueous Fe²⁺ concentrations after an equilibration period. The E_H values of Fe_(aq)²⁺-
116 goethite suspensions were measured using mediated potentiometry.³⁰ Specifically, 20 mL aqueous
117 solutions containing 25 mM KCl and 25 mM pH buffer in 20 mL borosilicate glass vials were spiked
118 with the Fe²⁺ stock to make initial Fe²⁺ concentrations ranging from 0.1 to 2.0 mM. For experiments
119 containing carbonate, the solution was spiked with an aliquot of 0.1 or 1 M NaHCO₃ stock solution
120 to make the desired concentrations (1 or 10 mM). We chose 10 mM as a maximum carbonate
121 concentration to avoid siderite (FeCO_{3(s)}) precipitation ($K_{sp} = 10^{-10.55}$) and to be consistent with past
122 studies.^{33, 39, 59} The pH 6.5 and 7.0 solutions were slightly oversaturated with respect to siderite. We
123 did not observe any loss of Fe²⁺ from solution that could be attributed to siderite formation in these
124 experiments, consistent with past studies^{33, 39, 59} and recent work that found siderite nucleation did

125 not occur under similar experimental conditions.⁵⁹ The solution pH was adjusted to 7.0 using 1 M
126 NaOH or HCl solution. Goethite solid was then added to the reactors to reach a mass loading of
127 1.0 g/L. The reactors were magnetically stirred. After 1 h, an aliquot of cyanomethyl viologen stock
128 solution was added to make a final mediator concentration of 10 μM . The reactors were sealed with
129 rubber septa and had negligible headspace to prevent carbonate degassing. After mixing in the dark
130 for 24 h, a small portion of each suspension was filtered through a 0.45 μm nylon syringe filter to
131 measure the final aqueous Fe^{2+} concentration.

132 The E_{H} values of $\text{Fe}_{(\text{aq})}^{2+}$ -goethite suspensions were measured using a Pt redox electrode
133 (Metrohm, part 6.0451.100) inside the glovebox. The data was sampled every 2 s until there was no
134 appreciable change in the measured E_{H} value over time. The final reading was reported as the E_{H}
135 value of the suspension. The electrode was periodically cleaned with 0.1 M HCl and calibrated with
136 quinhydrone-saturated pH buffer solutions at pH 4.0 and 7.0.^{28, 30} All measured E_{H} values were in
137 reference to Ag/AgCl and converted in reference to the standard hydrogen electrode (SHE) based
138 on the quinhydrone calibration values. The concentrations of total dissolved $\text{Fe}_{(\text{aq})}^{2+}$ were measured
139 using the 1,10-phenanthroline method.⁶⁰ The speciation of dissolved Fe^{2+} was calculated using the
140 thermodynamic database (thermo.Vdb) in Visual MINTEQ software, v3.1. We manually added
141 equilibria reactions for $\text{Fe}(\text{CO}_3)(\text{OH})^-$ and $\text{Fe}(\text{CO}_3)_2^-$, which are not in the MINTEQ
142 database.^{33, 55} The concentrations of $\text{Fe}(\text{H}_2\text{O})_6^{2+}$, which we refer to here as “free $\text{Fe}_{(\text{aq})}^{2+}$ ”, were
143 calculated using the chemical equilibrium model (Table S2) in Visual MINTEQ software. The
144 activity coefficients of free Fe^{2+} for each solution were calculated using the Davies model.

145 ***Nitrobenzene Reduction Experiments***

146 Nitrobenzene reduction experiments used the same reactor set-up as mediated potentiometry
147 measurements, except that no mediator was present. We varied the initial Fe^{2+} concentration (0.2

148 or 1.0 mM), carbonate concentration (0, 1, or 10 mM), goethite loading (0.25 - 3 g/L), and solution
149 pH (6.0, 6.5, or 7.0). After a 24 h equilibrium period between the goethite and aqueous Fe^{2+} , a small
150 aliquot was taken to measure the final $\text{Fe}_{(\text{aq})}^{2+}$ concentration. Nitrobenzene reduction experiments
151 started with the addition of an aliquot of 10 mM nitrobenzene stock solution made in deoxygenated
152 methanol to make an initial nitrobenzene concentration of $\sim 6 \mu\text{M}$. Each reactor was sealed with a
153 Teflon-lined septum and an aluminum crimp cap. At predetermined time intervals, samples were
154 taken and filtered through a $0.2 \mu\text{m}$ PTFE syringe filter. The sampling volume was minimized to
155 prevent CO_2 loss into the headspace. The concentrations of nitrobenzene and aniline were
156 measured using high pressure liquid chromatograph (HPLC) with a Supelcosil LC-18 column based
157 on previously established method.³⁰

158 ***Surface Charge and Particle Size Analysis***

159 The surface charges and aggregate sizes of $\text{Fe}_{(\text{aq})}^{2+}$ -goethite suspensions were measured by
160 electrophoretic and dynamic light scattering (Malvern Zetasizer Nano ZS), respectively. The reactors
161 were setup as described above, except that no mediator or nitrobenzene was added. The suspensions
162 contained 0.2 mM $\text{Fe}_{(\text{aq})}^{2+}$, 1 g/L goethite, 0-10 mM carbonate, 25 mM KCl, and 25 mM pH buffer.
163 We included Fe^{2+} in these measurements because preliminary measurements demonstrated that
164 $\text{Fe}_{(\text{aq})}^{2+}$ altered goethite aggregation in the presence of carbonate (data not shown). After a 24 h
165 equilibrium period, a portion of each suspension was transferred to cuvettes or zeta potential cells
166 that were sealed inside the glovebox, then taken out for subsequent analysis. The intensity weighted
167 mean hydrodynamic diameter was obtained from an autocorrelation function in a digital correlator
168 using the cumulants method.⁶¹ Laser diffraction (Mastersizer 3000) measurements were performed
169 under the same conditions, except that the mass loading of goethite was decreased to 0.05 g/L to

170 meet instrument requirements. The surface-weighted mean diameter was collected based on the Mie
171 scattering model.⁶²

172 **RESULTS AND DISCUSSION**

173 *Effect of Carbonate on Nitrobenzene Reduction Kinetics*

174 We examined the effect of carbonate on nitrobenzene reduction rates by goethite-bound Fe²⁺ at
175 different pH values, goethite mass loadings, and initial Fe_(aq)²⁺ concentrations (**Table S3**). In all
176 experiments, nitrobenzene disappearance followed pseudo-first-order kinetics, consistent with past
177 studies:^{28, 63}

$$178 \quad \frac{d[\text{NB}]}{dt} = -k_{\text{obs}}[\text{NB}] \quad (3)$$

179 where [NB] is the concentration of nitrobenzene (μM), and k_{obs} is the observed pseudo-first-order
180 reduction rate constant (h^{-1}). The presence of carbonate slowed the rate of nitrobenzene
181 disappearance, with k_{obs} values decreasing from $25.8 \pm 0.8 \text{ h}^{-1}$ (no carbonate) to $7.1 \pm 0.4 \text{ h}^{-1}$ (10
182 mM total carbonate) at pH 7.0, 0.2 mM initial Fe_(aq)²⁺, and 0.5 g/L goethite (**Figure 1**). Nitrobenzene
183 reduction was coupled to aniline production, and a stoichiometric amount of aniline was produced
184 when the reaction was provided sufficient time to proceed to completion (**Figure S3**). In control
185 experiments lacking goethite, no nitrobenzene disappearance or aniline production occurred over a
186 24-hour period regardless of the carbonate concentration (**Figure S4**), confirming that goethite-
187 bound Fe²⁺ was the responsible species for nitrobenzene reduction, rather than dissolved Fe²⁺
188 species.^{30, 64}

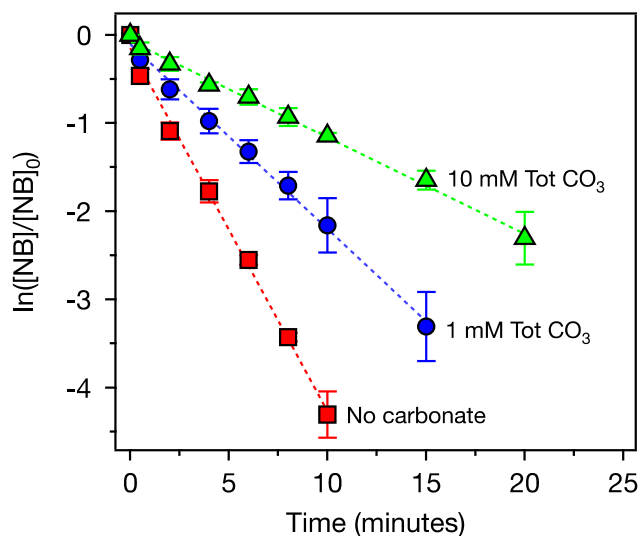


Figure 1. Nitrobenzene (NB) reduction in suspensions containing goethite and aqueous Fe^{2+} at varied total carbonate concentrations. Reactor conditions: 0.2 mM total Fe^{2+} , 0.5 g/L goethite, 25 mM MOPS buffer, 25 mM KCl, and pH = 7.0. The reactors were equilibrated for 24 h prior to the addition of 6 μM nitrobenzene. Error bars represent the two values measured from duplicate reactors, and points represent the average. Straight lines represent the linear fits with pseudo-first-order kinetic model.

189 We compared measured k_{obs} values with reported values from the literature. In the absence
 190 of carbonate, the k_{obs} value ($25.8 \pm 0.8 \text{ h}^{-1}$), collected with 0.2 mM total Fe^{2+} and 0.5 g/L goethite,
 191 agreed well with our previously reported value ($32.3 \pm 0.7 \text{ h}^{-1}$) collected under similar experimental
 192 conditions (0.5 mM total Fe^{2+} and 1 g/L goethite).²⁸ We previously found this value was consistent
 193 with those compiled from several other studies (**Figure S1A**).²⁸ In the presence of carbonate,
 194 however, our reported k_{obs} value ($7.1 \pm 0.4 \text{ h}^{-1}$) was approximately 8 times greater than a value
 195 reported in a recent study that used similar experimental conditions with 4-chloro-nitrobenzene (k_{obs}
 196 = $0.96 \pm 0.09 \text{ h}^{-1}$).³⁹ A table detailing the experimental conditions of the two studies is in the
 197 Supporting Information (**Table S4**). The substantially larger k_{obs} value in our study was surprising
 198 given that the goethite surface area loading and the initial $\text{Fe}_{(\text{aq})}^{2+}$ concentration were higher in the
 199 cited study³⁹ (45 m^2/L and 0.5 mM) than this study (18 m^2/L and 0.2 mM). We examined if this
 200 difference was due to the pH buffer (i.e., MOPS) used in our experiments.³¹ Our solution contained

201 25 mM MOPS and 10 mM total carbonate, whereas the former study used only 10 mM total
202 carbonate. When we performed a nitrobenzene reduction experiment without MOPS, the k_{obs} value
203 (6.5 h^{-1}) was similar to what we observed when 25 mM MOPS was present (7.6 h^{-1}) (**Figure S5**),
204 indicating that the presence of MOPS could not explain the difference in nitrobenzene reduction
205 kinetics. We suspect that the discrepancy in k_{obs} values between the studies may be due to the former
206 study using a much higher initial nitrobenzene concentration ($50 \mu\text{M}$)³⁹ than what we used ($\sim 6 \mu\text{M}$).
207 We observed that high initial nitrobenzene concentrations in the former study prominently
208 decreased the solution pH over the course of the reaction because of insufficient buffer capacity
209 offered by 10 mM carbonate, as twelve protons are generated to completely reduce one nitrobenzene
210 molecule to one aniline molecule by Fe^{2+} bound to goethite.²⁸

211 We explored possible explanations for why carbonate decreased nitrobenzene reduction
212 rates in our experiments. We first examined if carbonate slowed nitrobenzene reduction rates by
213 competing with Fe^{2+} for sorption sites at the goethite surface, as carbonate is known to form surface
214 complexes on goethite at circumneutral pH values.^{33, 65, 66} We compared the extent of Fe^{2+} uptake
215 on the goethite surfaces in the experiments from **Figure 1** and in additional experiments with
216 different goethite mass loadings at pH 7.0 (**Table S3**). The oxide-bound Fe^{2+} loadings for 200 μM
217 initial $\text{Fe}_{(\text{aq})}^{2+}$ were indistinguishable at the different total carbonate concentrations (0 mM: 133 ± 54
218 $\mu\text{mol/g}$, $n = 6$; 1 mM: $130 \pm 16 \mu\text{mol/g}$, $n = 6$; 10 mM: $132 \pm 33 \mu\text{mol/g}$, $n = 7$), indicating that
219 carbonate did not inhibit Fe^{2+} uptake by goethite at 0.2 mM total Fe^{2+} . We did, however, observe
220 that carbonate modestly inhibited Fe^{2+} uptake at higher Fe^{2+} concentrations ($\geq 0.5 \text{ mM}$) at pH 7
221 (**Figure 2**). Note a prior study found carbonate significantly inhibited Fe^{2+} sorption on goethite at pH
222 7.0 under similar goethite surface area loadings and initial Fe^{2+} concentrations.³³ We were unable to
223 reproduce their observation, even when we replicated their experiment (**Figure S6**). Unfortunately,

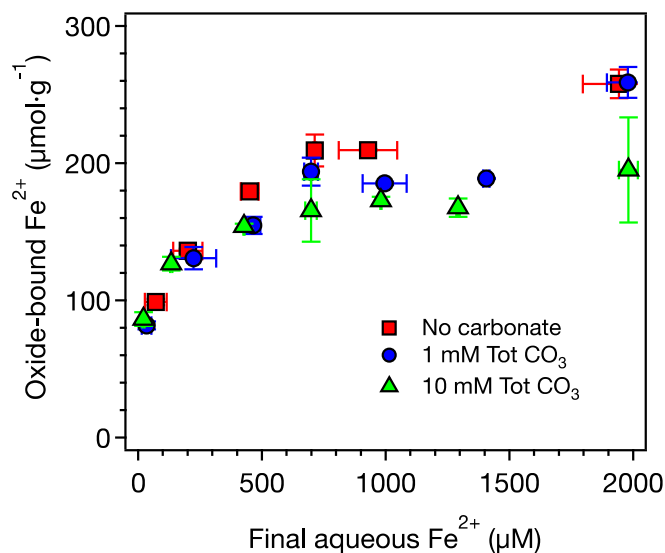


Figure 2. Impact of carbonate on $\text{Fe}_{(\text{aq})}^{2+}$ uptake by goethite at pH 7.0 with a 24-hour equilibration time. Error bars represent the two values measured from duplicate reactors, and points represent the average. Experimental conditions: 1 g/L goethite, 25 mM KCl, 25 mM MOPS buffer.

224 we were unable to identify why our results differed from those in the previous work. As a result of
 225 our experiments, we ruled out the possibility that nitrobenzene reduction was slowed by carbonate
 226 because it inhibited Fe^{2+} uptake (i.e., decreased the number of reactive Fe^{2+} sites), based on the lack
 227 of evidence for inhibition at 0.2 mM Fe^{2+} . This finding led us to examine how carbonate influenced
 228 E_{H} values of goethite-bound Fe^{2+} .

229 *Effect of Carbonate on E_{H} Values*

230 For each data point in **Figure 2**, we measured the E_{H} value of the suspension using mediated
 231 potentiometry. Carbonate had a negligible effect on E_{H} values as a function of the concentration of
 232 $\text{Fe}(\text{H}_2\text{O})_6^{2+}$ (i.e., “free $\text{Fe}_{(\text{aq})}^{2+}$ ”) at pH 7 (**Figure 3**).^{28, 67, 68} Note that we transition here from
 233 considering the data in terms of total dissolved Fe^{2+} to free $\text{Fe}_{(\text{aq})}^{2+}$ because the Nernst equation
 234 requires consideration of a specific Fe^{2+} species. In the presence of carbonate, a portion of the
 235 dissolved Fe^{2+} complexes with carbonate to form $\text{Fe}(\text{CO}_3)(\text{H}_2\text{O})_5^{0}_{(\text{aq})}$ (i.e., FeCO_3^0) and, to a lesser

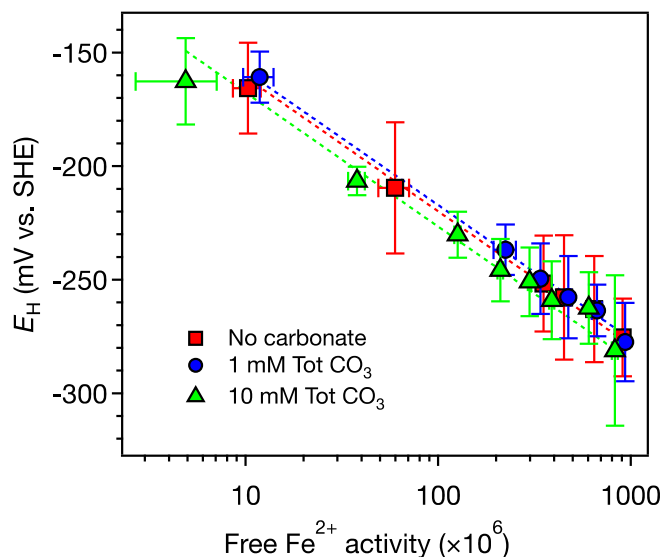


Figure 3. Impact of carbonate on reduction potentials of goethite suspensions as a function of free $\text{Fe}_{(\text{aq})}^{2+}$ activity at pH 7.0. Error bars represent the two values measured from duplicate reactors, and points represent the average. Experimental conditions: 1 g/L goethite, 25 mM KCl, 25 mM MOPS buffer, and 10 μM mediator. Dash lines represent data fits using eq. 4.

236 degree, $\text{Fe}(\text{HCO}_3)(\text{H}_2\text{O})_{5(\text{aq})}^+$ (i.e., FeHCO_3^+).⁵⁵ In the presence of 10 mM total carbonate at pH 7,
 237 approximately 35% of total aqueous Fe^{2+} will be present as FeCO_3^0 or FeHCO_3^+ (and 3.5% at 1 mM
 238 total carbonate), which was calculated based on chemical equilibrium model (**Table S2**) in Visual
 239 MINTEQ software, V3.1 (**Figure S7**).⁵⁵

240 Prior work has shown aqueous suspensions of goethite and $\text{Fe}_{(\text{aq})}^{2+}$ reach thermodynamic
 241 equilibrium and can be described by the half reaction shown in eq. 2 and the corresponding Nernst
 242 equation:³⁰

$$243 \quad E_{\text{H}} = E_{\text{H}}^0 - \frac{RT}{F} \ln \{ \text{Fe}_{(\text{aq})}^{2+} \} + 3 \frac{RT}{F} \ln \{ \text{H}^+ \} \quad (4)$$

244 where $\text{Fe}_{(\text{aq})}^{2+}$ is $\text{Fe}(\text{H}_2\text{O})_{6(\text{aq})}^{2+}$, R is the ideal gas constant, T is temperature, and F is Faraday's constant.

245 At room temperature (298 K), the expression simplifies to:

$$246 \quad E_{\text{H}} = E_{\text{H}}^0 - 0.059\text{V} \cdot \log \{ \text{Fe}_{(\text{aq})}^{2+} \} - 0.177\text{V} \cdot \text{pH} \quad (5)$$

247 Regardless of carbonate concentrations, the measured E_H values were well fit by eq. 5 when assuming
248 the theoretical slope value for $\text{Fe}_{(\text{aq})}^{2+}$ activity (**Figure 3**), confirming that goethite and aqueous Fe^{2+}
249 reached thermodynamic equilibrium. Although the free $\text{Fe}_{(\text{aq})}^{2+}$ concentration decreases by 35% at 10
250 mM carbonate because of complexation reactions (**Figure S7**), calculations based on eq. 4 shows
251 that such a change only varies E_H values by 10 mV, which is consistent with minor change in E_H
252 values experimentally observed (**Figure 3**). The fitted E_H^0 values of α - $\text{FeOOH}_{(\text{s})}/\text{Fe}_{(\text{aq})}^{2+}$ redox couple
253 in **Figure 3** are 783 ± 1 mV vs. SHE (no carbonate), 786 ± 1 mV (1 mM total carbonate), and $775 \pm$
254 2 mV (10 mM). The values agree well with previously reported values for goethite (800 ± 3 mV²⁸
255 and 768 ± 1 mV³⁰), indicating that carbonate did not affect the α - $\text{FeOOH}_{(\text{s})}/\text{Fe}_{(\text{aq})}^{2+}$ half-reaction.
256 We used the average E_H^0 value (781 mV) and eq. 5 to calculate E_H values in all subsequent
257 experiments.

258 *Relationship between E_H Values and Nitrobenzene Reduction Kinetics*

259 We examined how nitrobenzene reduction kinetics varied as a function of solution E_H and total
260 carbonate concentration (data tabulated in **Table S3**). We surface-area-normalized the k_{obs} values
261 following a standard convention:^{28, 69, 70}

$$262 \quad k_{\text{SA}} = \frac{k_{\text{obs}}}{A} \quad (6)$$

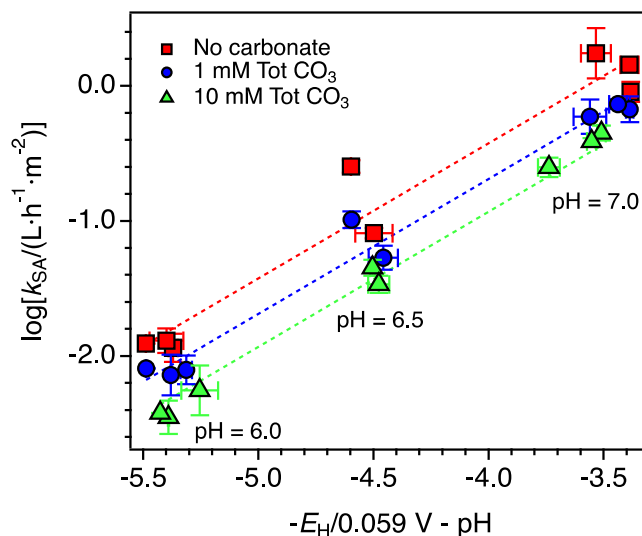


Figure 4. Linear free energy relationship between $\log(k_{SA})$ values and E_H and pH values. The slope of the line was held at 1 during the least-square linear regression. Error bars represent the two values measured from duplicate reactors, and points represent the average. The dash lines represent the linear fits: $r^2 = 0.95$ (red), 0.98 (blue), and 0.99 (green).

263 where A is the surface area of goethite (m^2/L) in the suspensions, which is calculated by multiplying
 264 the goethite BET specific surface area (m^2/g) by the goethite mass loading (g/L). The k_{SA} values
 265 consequently have units of $L \cdot h^{-1} \cdot m^{-2}$. We graphed $\log(k_{SA})$ values as a function of E_H and pH values
 266 based on the linear free energy relationship shown in **Figure S1A** and expressed in eq. 1 (**Figure 4**),
 267 with the slope terms (a and b) held constant at -1 .²⁸ Floating both the slopes and y-intercepts during
 268 fitting yielded slopes close to 1 (no carbonate: 1.00 ± 0.10 , 1 mM total carbonate: 0.99 ± 0.06 , 10
 269 mM total carbonate: 1.09 ± 0.02 ; **Figure S8**). Note the data points cluster separately with respect to
 270 pH because the pH has a substantial impact on the thermodynamic driving force of nitrobenzene
 271 reduction by oxide-bound Fe^{2+} .²⁸ Plotting the data in this way clearly revealed that carbonate did not
 272 affect the slope of the free energy relationship, indicating that carbonate did not change the
 273 mechanisms and rate-limiting step of the redox reaction between nitrobenzene and oxide-bound
 274 Fe^{2+} .²⁸ We further confirmed that carbonate did not affect the slope in the free energy relationship
 275 by performing a 1:1 correlation of $\log(k_{SA})$ values in carbonate-present vs. carbonate-free systems,

276 which yielded two straight line with slope values also equal to 1 within error (i.e., 1.02 ± 0.06 and
277 0.98 ± 0.08 , **Figure S9**).¹⁰

278 Carbonate did, however, change the y-intercept of the linear free energy relationship (i.e.,
279 the c term in eq. 1), with c values lower at higher carbonate concentrations (when the slope was held
280 at 1): 3.57 ± 0.08 (no carbonate), 3.31 ± 0.05 (1 mM total carbonate), and 3.07 ± 0.03 (10 mM).
281 These values reflect an average decrease in k_{SA} by a factor of 1.9 ± 0.8 in 1 mM total carbonate and
282 a factor of 3.3 ± 1.1 in 10 mM total carbonate, relative to 0 mM total carbonate. This trend indicates
283 that carbonate decreased the number of reactive sites and/or the frequency of interactions between
284 nitrobenzene and reactive sites because we did not observe any-change in the E_H^0 values (**Figure 3**).
285 This observation led us to determine how carbonate influenced the reactive surface area of goethite
286 by examining its role in particle aggregation.

287 ***Role of Carbonate in Goethite Aggregation***

288 To determine if carbonate altered the reactive surface area of goethite, we investigated how the
289 aggregation state of goethite and aqueous Fe^{2+} suspensions changed upon the addition of carbonate.
290 The mean hydrodynamic diameters of goethite aggregates became larger when carbonate was added,
291 as evidenced by dynamic light scattering (DLS) measurements (**Figure 5A**). At pH 6.0, DLS
292 measurements indicated that the mean hydrodynamic diameter of the goethite aggregates increased
293 from $1.26 \pm 0.02 \mu m$ (0 mM total carbonate) to $4.8 \pm 0.7 \mu m$ (10 mM) (**Figure 5A**). Carbonate also
294 caused goethite to aggregate at pH 6.5 (0 mM: $2.6 \pm 0.3 \mu m$, 10 mM: $6.2 \pm 0.5 \mu m$) and pH 7.0 (0
295 mM: $3.6 \pm 0.7 \mu m$, 10 mM: $5.5 \pm 0.7 \mu m$). Note that calculated hydrodynamic diameters from DLS
296 measurements made at pH 6.5 and 7.0 may have contained some error, as the diameters approached
297 the quantitative detection limit of DLS ($\sim 10 \mu m$) and sedimentation was visually apparent during the
298 measurements.³¹ Attempts to decrease sedimentation and aggregate sizes by decreasing the goethite

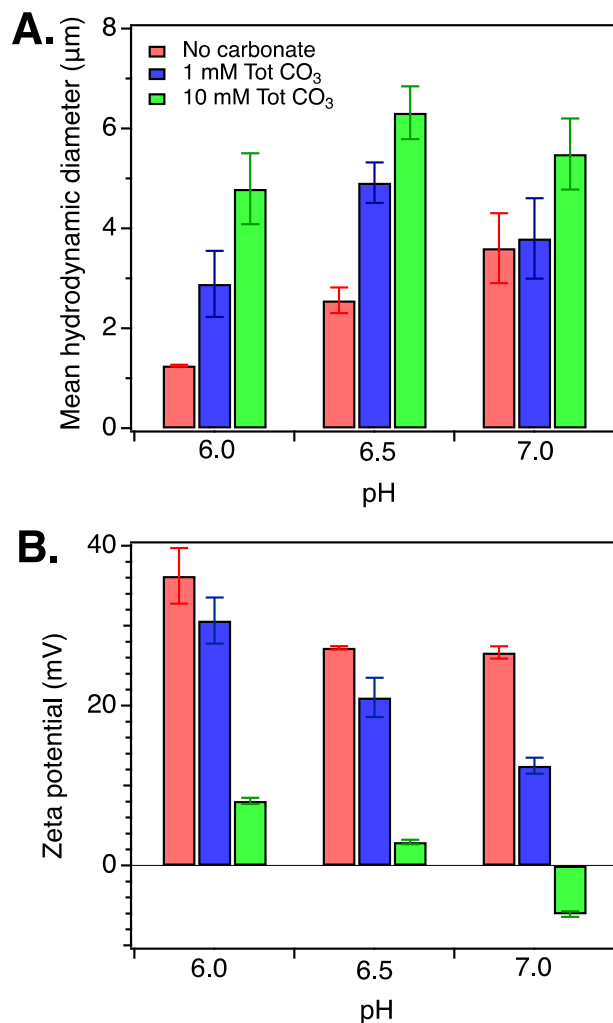


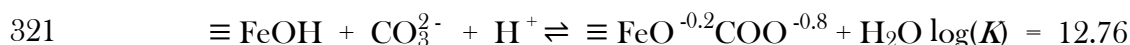
Figure 5. Impact of carbonate on the mean hydrodynamic diameters (A) and zeta potentials (B) of goethite in the presence of $\text{Fe}_{(\text{aq})}^{2+}$ at different pH values. Error bars represent standard deviations from triplicate measurements. Experimental conditions: 1 g/L goethite, 0.2 mM $\text{Fe}_{(\text{aq})}^{2+}$, 25 mM KCl, and 25 mM MES or MOPS buffer.

299 loading in solution were unsuccessful (data not shown). Despite the potential for quantitative artifacts
300 in the DLS analyses, the data clearly demonstrated that carbonate increased goethite aggregations.

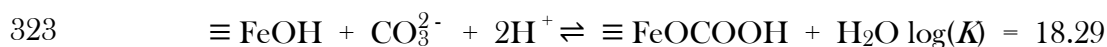
301 We also measured goethite aggregation state using laser diffraction, which has a wider
302 detection range (10 nm - 3500 μm),⁶² but requires the samples to be exposed to air during analysis.
303 These measurements confirmed that carbonate induced aggregation (Figure S10). At pH 6.0, the
304 mean diameter of goethite aggregates increased from 2.4 ± 0.1 (0 mM total carbonate) to 5.0 ± 0.1

305 μm (10 mM total carbonate), consistent with the DLS results. Similarly, laser diffractions
 306 measurements also indicated that carbonate induced goethite aggregation at pH 6.5 (0 mM: $3.3 \pm$
 307 0.1 , 10 mM: 4.9 ± 0.1) and pH 7.0 (0 mM: $3.0 \pm 0.2 \mu\text{m}$, 10 mM: $4.3 \pm 0.1 \mu\text{m}$), although the
 308 magnitude of the effect was smaller than what we measured with DLS. We suspect the laser
 309 diffraction measurements may have been affected by Fe^{2+} oxidation due to air exposure during
 310 analysis. Prior work found that Fe^{2+} oxidation by oxygen changes the surface charge and aggregation
 311 states of goethite.³⁹

312 We examined if the reason carbonate increased goethite aggregation was that it formed
 313 surface complexes on the goethite surface that altered the particles' surface charge.^{33, 71} We tested
 314 this hypothesis by performing zeta potential measurements on the suspensions used for DLS
 315 experiments (**Figure 5B**). Over pH 6.0 to 7.0, carbonate lowered the surface charge of goethite,
 316 bringing it closer to zero thus favoring particle aggregation by decreasing interparticle repulsive forces.
 317 The point of zero charge of goethite has been reported to be approximately 9.0,⁷² but the presence
 318 of 10 mM carbonate lowered it to a value between 6.5 to 7.0 (**Figure 5B**). Prior work has reported
 319 the following inner-sphere surface complexation reactions of carbonate interacting with goethite
 320 surfaces:³³



322 (7)



324 (8)

325 In addition, carbonate likely formed outer-sphere complexes in the double layer of goethite particles
 326 through electrostatic interaction and neutralized positively charged goethite surface. Our results are

327 consistent with carbonate forming surface complexes on goethite and inducing aggregation, yet
328 interestingly our earlier results in **Figure 2** indicated that Fe^{2+} and carbonate did not compete for
329 sorption sites with 0.2 mM total Fe^{2+} . Given the strong evidence for interfacial electron-transfer
330 between Fe^{2+} and iron oxides, we speculate that this observation may be a result of Fe^{2+} uptake extent
331 being controlled by the redox properties of the iron oxide as opposed to surface complexation
332 associated with the number of surface sites.⁷¹⁻⁷³

333 ***Correcting the Reactive Surface Area of Goethite***

334 As discussed above, the linear free energy relationships in **Figure 4** were developed using a k_{SA} value
335 that was calculated based on the BET surface area of dry goethite (eq. 5). However, the actual
336 reactive surface area of goethite in aqueous suspensions appeared to vary with respect to the total
337 carbonate concentration due to aggregation. To account for aggregation in the free energy
338 relationship, we normalized nitrobenzene reduction rate constant (k_{obs}) with the calculated goethite
339 specific surface area in aqueous suspension from DLS and laser diffraction measurements. This
340 normalization required us to make an approximation that the goethite aggregates, which likely
341 consisted of loosely and irregularly bound rod-shaped particles,³⁸ could be described as spherical
342 particles. This approximation would be valid if the actual reactive surface area of the aggregate is
343 linearly proportional to the calculated surface area when assuming the aggregates are spherical. Using
344 this approximation, we calculated the geometric specific surface area (SSA_{aq}) based on the mean
345 diameters (d) of equivalent spheres of goethite:^{73, 74}

$$346 \quad \text{SSA}_{\text{aq}} = \frac{4\pi\left(\frac{d}{2}\right)^2}{\rho \frac{4}{3}\pi\left(\frac{d}{2}\right)^3} = \frac{6}{\rho d} \quad (9)$$

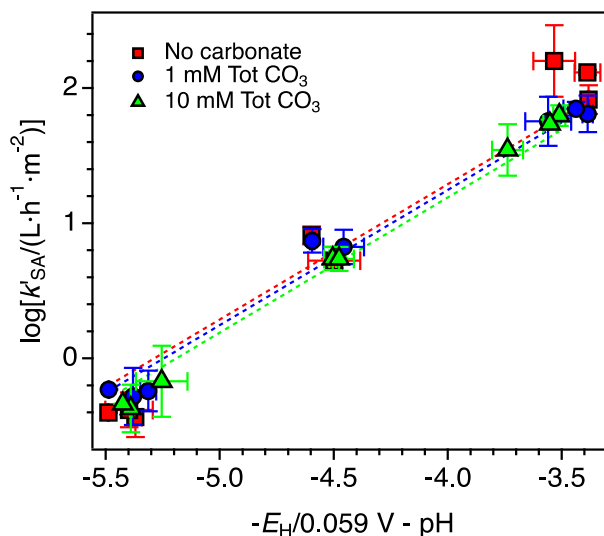


Figure 6. Impact of carbonate on the logarithms of the calibrated surface-area-normalized reaction rate constants ($\log(k'_{SA})$) based on DLS results as a function of E_H and pH values of $Fe_{(aq)}^{2+}$ -goethite suspension for nitrobenzene reduction. Dashed lines represent the linear fits: $r^2 = 0.94$ (red), 0.98 (blue), and 0.99 (green). The slopes were held at 1 during fitting. When the slopes were allowed to float, they reached values close to 1, with the small deviations attributed to experimental error.

347 where ρ represents the density of goethite (4.26 g/cm^3).⁷⁵ The calculated SSA_{aq} values from DLS
 348 and laser diffraction ranged from 0.21 to $1.13 \text{ m}^2/\text{g}$, depending on the pH and total carbonate
 349 concentrations. The SSA_{aq} values were much lower than the BET specific surface area value
 350 measured for the dry particles ($36 \text{ m}^2/\text{g}$), which was likely due to the aggregation and our simplistic
 351 approximation that the aggregates were spherical.

352 We then re-adjusted our linear free energy relationship by calculating the logarithm of the
 353 calibrated surface-area-normalized reaction rate constant ($\log(k'_{SA})$):

$$354 \quad \log(k'_{SA}) = \log\left(\frac{k_{obs}}{SSA_{aq} \cdot m_L}\right) \quad (10)$$

355 where m_L is mass loading (g/L) of goethite. We graphed $\log(k'_{SA})$ values as a function of E_H and pH
 356 values based on the linear free energy relationship (eq.1). After the calibration based on DLS results,
 357 the scattered data points in **Figure 4** closely converged for different carbonate concentrations (**Figure**

358 **6**), which was quantitatively reflected by the similarity among the fitted y-intercepts (*c* term): $5.29 \pm$
359 0.10 (0 mM), 5.25 ± 0.04 (1 mM), and 5.19 ± 0.04 (10 mM). Calibration based on laser diffraction
360 results also highly reduced scatter among the data (**Figure S11**), although they converged to a lesser
361 extent. These results indicate that the loss of the reactive surface area due to goethite aggregation was
362 the primary reason that nitrobenzene reduction slowed in the presence of carbonate. Therefore, we
363 concluded that the main mechanism by which carbonate slows nitrobenzene reduction by Fe^{2+} -
364 bound to goethite is via particle aggregation caused by carbonate forming surface complexes on the
365 goethite surface that decrease the positive surface charge of goethite.

366 *Environmental implications*

367 Our results indicate that the predominant way in which carbonate alters the reduction rates of
368 nitroaromatic compounds by oxide-bound Fe^{2+} is by changing particulate aggregation state.
369 Carbonate increased goethite aggregation, which decreased the number of reactive sites on goethite
370 surfaces. We did not observe any evidence suggesting that carbonate affected the nitrobenzene
371 reduction mechanism, which would have changed the slope of the linear free energy relationship.
372 The effect that carbonate has on iron oxide particle aggregation will be highly specific to the iron
373 oxide present because aggregation behavior depends on the point of zero charge of an iron oxides,
374 which is oxide-specific.⁷⁵ Reported point of zero charge values for goethite range between 8.9 - 9.4.⁷⁵
375 Other iron oxides have far lower point of zero charges, such as magnetite (6.3 - 7.1) and
376 lepidocrocite (6.7 - 7.45).⁷⁵ Given the differences in point of zero charge, iron oxides likely have
377 distinctive surface charges under environmentally relevant conditions, which affects surface
378 complexation of carbonate on iron oxides. Consequently, carbonate will likely affect their
379 aggregation behavior differently.

380 More generally, our results offer evidence to support the use of free energy relationships to
381 understand how groundwater constituents alter pollutant reduction rates by oxide-bound Fe^{2+}
382 mechanistically. By constructing a free energy relationship that relates reduction rates to the
383 thermodynamic driving force of the reaction, one can differentiate between how a groundwater
384 constituent may change a reaction pathway (as evidenced by a change in the slope of the relationship)
385 or how it changes the number of reactive sites or the Fe^{2+} oxidation product that forms (as evidenced
386 by a change to the y-intercept). Coupling this analysis with E_{H} measurements could, for example,
387 allow one to discriminate among possible reasons that humic acids alter nitroaromatic reduction
388 rates by oxide-bound Fe^{2+} , which has proven to be a difficult task.⁵¹⁻⁵³ Humic acid may alter pollutant
389 reduction rates by aggregating particles,^{38, 76} complexing aqueous Fe^{2+} ,^{77, 78} changing Fe^{2+} oxidation
390 products,⁷⁷ and/or by serving as electron shuttles.⁵¹ Coupling E_{H} measurements with conventionally
391 used approaches may allow researchers to discriminate among these possibilities for other classes of
392 contaminants as well, as was recently shown for chlorinated solvents reacted with reduced natural
393 sediments.¹⁶

394 **ASSOCIATED CONTENT**

395 The Supporting Information include compiled data from the literature, the XRD pattern of goethite,
396 the impact of carbonate on E_{H} values, the goethite particle sizes and nitrobenzene reduction, the
397 impact of MOPS buffer on nitrobenzene reduction, and the predominance diagrams of Fe^{2+} species.

398 **ACKNOWLEDGEMENT**

399 The study was supported by U.S. National Science Foundation Program (CHE-1807703 to CAG)
400 Swiss National Science Foundation (Grant 200021_149283 to TBH).

401 **REFERENCES**

- 402 1. Eary, L.; Rai, D., Chromate removal from aqueous wastes by reduction with ferrous
403 ion. *Environmental Science & Technology* **1988**, *22*, (8), 972-977.
- 404 2. Buerge, I. J.; Hug, S. J., Influence of mineral surfaces on chromium (VI) reduction
405 by iron (II). *Environmental Science & Technology* **1999**, *33*, (23), 4285-4291.
- 406 3. Latta, D. E.; Gorski, C. A.; Boyanov, M. I.; O'Loughlin, E. J.; Kemner, K. M.; Scherer,
407 M. M., Influence of magnetite stoichiometry on UVI reduction. *Environmental
408 Science & Technology* **2012**, *46*, (2), 778-786.
- 409 4. Myneni, S. C. B.; Tokunaga, T. K.; Brown, G., Abiotic selenium redox
410 transformations in the presence of Fe (II, III) oxides. *Science* **1997**, *278*, (5340), 1106-
411 1109.
- 412 5. Amonette, J. E.; Workman, D. J.; Kennedy, D. W.; Fruchter, J. S.; Gorby, Y. A.,
413 Dechlorination of carbon tetrachloride by Fe (II) associated with goethite. *Environ.
414 Sci. Technol.* **2000**, *34*, (21), 4606-4613.
- 415 6. Pecher, K.; Haderlein, S. B.; Schwarzenbach, R. P., Reduction of polyhalogenated
416 methanes by surface-bound Fe (II) in aqueous suspensions of iron oxides. *Environ.
417 Sci. Technol.* **2002**, *36*, (8), 1734-1741.
- 418 7. Strathmann, T. J.; Stone, A. T., Mineral surface catalysis of reactions between FeII
419 and oxime carbamate pesticides. *Geochim. Cosmochim. Acta* **2003**, *67*, (15), 2775-
420 2791.
- 421 8. Li, X.; Chen, Y.; Zhang, H., Reduction of nitrogen-oxygen containing compounds
422 (NOCs) by surface-associated Fe (II) and comparison with soluble Fe (II) complexes.
423 *Chemical Engineering Journal* **2019**, *370*, 782-791.
- 424 9. Elsner, M.; Schwarzenbach, R. P.; Haderlein, S., Reactivity of Fe(II)-Bearing Minerals
425 toward Reductive Transformation of Organic Contaminants. *Environmental Science
426 & Technology* **2004**, *38*, 799-807.
- 427 10. Tratnyek, P. G.; Weber, E. J.; Schwarzenbach, R. P., Quantitative structure-activity
428 relationships for chemical reductions of organic contaminants. *Environmental
429 Toxicology and Chemistry: An International Journal* **2003**, *22*, (8), 1733-1742.
- 430 11. Amstatter, K.; Borch, T.; Larese-Casanova, P.; Kappler, A., Redox transformation
431 of arsenic by Fe (II)-activated goethite (α -FeOOH). *Environmental science &
432 technology* **2010**, *44*, (1), 102-108.
- 433 12. Jeon, B.-H.; Dempsey, B. A.; Burgos, W. D.; Barnett, M. O.; Roden, E. E., Chemical
434 reduction of U (VI) by Fe (II) at the solid- water interface using natural and synthetic
435 Fe (III) oxides. *Environmental Science & Technology* **2005**, *39*, (15), 5642-5649.

- 436 13. Melton, E. D.; Swanner, E. D.; Behrens, S.; Schmidt, C.; Kappler, A., The interplay
437 of microbially mediated and abiotic reactions in the biogeochemical Fe cycle. *Nature*
438 *Reviews Microbiology* **2014**, *12*, (12), 797-808.
- 439 14. Fan, D.; Bradley, M. J.; Hinkle, A. W.; Johnson, R. L.; Tratnyek, P. G., Chemical
440 reactivity probes for assessing abiotic natural attenuation by reducing iron minerals.
441 *Environmental science & technology* **2016**, *50*, (4), 1868-1876.
- 442 15. Bussan, A. L.; Strathmann, T. J., Influence of organic ligands on the reduction of
443 polyhalogenated alkanes by iron (II). *Environmental science & technology* **2007**, *41*,
444 (19), 6740-6747.
- 445 16. Kocur, C. M.; Fan, D.; Tratnyek, P. G.; Johnson, R. L., Predicting Abiotic Reduction
446 Rates Using Cryogenically Collected Soil Cores and Mediated Reduction Potential
447 Measurements. *Environmental Science & Technology Letters* **2019**.
- 448 17. Wilkin, R. T.; Su, C.; Ford, R. G.; Paul, C. J., Chromium-removal processes during
449 groundwater remediation by a zerovalent iron permeable reactive barrier.
450 *Environmental science & technology* **2005**, *39*, (12), 4599-4605.
- 451 18. Liang, S.; Kao, C.; Kuo, Y.; Chen, K.; Yang, B., In situ oxidation of petroleum-
452 hydrocarbon contaminated groundwater using passive ISCO system. *water research*
453 **2011**, *45*, (8), 2496-2506.
- 454 19. Amonette, J. E.; Workman, D. J.; Kennedy, D. W.; Fruchter, J. S.; Gorby, Y. A.,
455 Dechlorination of Carbon Tetrachloride by Fe(II) Associated with Goethite.
456 *Environmental Science & Technology* **2000**, *34*, (21), 4606-4613.
- 457 20. Strathmann, T. J.; Stone, A. T., Mineral surface catalysis of reactions between Fe(II)
458 and oxime carbamate pesticides. *Geochimica Et Cosmochimica Acta* **2003**, *67*, (15),
459 2775-2791.
- 460 21. Klausen, J.; Trober, S. P.; Haderlein, S. B.; Schwarzenbach, R. P., Reduction of
461 substituted nitrobenzenes by Fe(II) in aqueous mineral suspensions. *Environmental*
462 *Science & Technology* **1995**, *29*, (9), 2396-2404.
- 463 22. Rügge, K.; Hofstetter, T. B.; Haderlein, S. B.; Bjerg, P. L.; Knudsen, S.; Zraunig, C.;
464 Mosbæk, H.; Christensen, T. H., Characterization of Predominant Reductants in an
465 Anaerobic Leachate-Contaminated Aquifer by Nitroaromatic Probe Compounds.
466 *Environmental Science & Technology* **1998**, *32*, (1), 23-31.
- 467 23. Pecher, K.; Haderlein, S. B.; Schwarzenbach, R. P., Reduction of polyhalogenated
468 methanes by surface-bound Fe(II) in aqueous suspensions of iron oxides.
469 *Environmental Science & Technology* **2002**, *36*, (8), 1734-1741.
- 470 24. Cui, D.; Eriksen, T. E., Reduction of pertechnetate by ferrous iron in solution:
471 Influence of sorbed and precipitated Fe (II). *Environmental science & technology*
472 **1996**, *30*, (7), 2259-2262.

- 473 25. Liger, E.; Charlet, L.; Van Cappellen, P., Surface catalysis of uranium(VI) reduction
474 by iron(II). *Geochimica et Cosmochimica Acta* **1999**, *63*, (19-20), 2939-2955.
- 475 26. Colón, D.; Weber, E. J.; Anderson, J. L., QSAR Study of the Reduction of
476 Nitroaromatics by Fe(II) Species. *Environmental Science & Technology* **2006**, *40*,
477 (16), 4976-4982.
- 478 27. Jones, A. M.; Kinsela, A. S.; Collins, R. N.; Waite, T. D., The reduction of 4-
479 chloronitrobenzene by Fe(II)-Fe(III) oxide systems - correlations with reduction
480 potential and inhibition by silicate. *Journal of Hazardous Materials* **2016**, *320*, 143-
481 149.
- 482 28. Stewart, S. M.; Hofstetter, T. B.; Joshi, P.; Gorski, C. A., Linking thermodynamics to
483 pollutant reduction kinetics by Fe²⁺ bound to iron oxides. *Environmental science &*
484 *technology* **2018**, *52*, (10), 5600-5609.
- 485 29. Strehlau, J. H.; Schultz, J. D.; Vindedahl, A. M.; Arnold, W. A.; Penn, R. L., Effect
486 of nonreactive kaolinite on 4-chloronitrobenzene reduction by Fe (II) in goethite-
487 kaolinite heterogeneous suspensions. *Environmental Science: Nano* **2017**, *4*, (2), 325-
488 334.
- 489 30. Gorski, C. A.; Edwards, R.; Sander, M.; Hofstetter, T. B.; Stewart, S. M.,
490 Thermodynamic characterization of iron oxide-aqueous Fe²⁺ redox couples.
491 *Environmental science & technology* **2016**, *50*, (16), 8538-8547.
- 492 31. Stemig, A. M.; Do, T. A.; Yuwono, V. M.; Arnold, W. A.; Penn, R. L., Goethite
493 nanoparticle aggregation: effects of buffers, metal ions, and 4-chloronitrobenzene
494 reduction. *Environmental Science: Nano* **2014**, *1*, (5), 478-487.
- 495 32. Chun, C. L.; Penn, R. L.; Arnold, W. A., Kinetic and microscopic studies of reductive
496 transformations of organic contaminants on goethite. *Environmental Science &*
497 *Technology* **2006**, *40*, (10), 3299-3304.
- 498 33. Vikesland, P. J.; Valentine, R. L., Iron oxide surface-catalyzed oxidation of ferrous
499 iron by monochloramine: Implications of oxide type and carbonate on reactivity.
500 *Environmental science & technology* **2002**, *36*, (3), 512-519.
- 501 34. Liger, E.; Charlet, L.; Van Cappellen, P., Surface catalysis of uranium (VI) reduction
502 by iron (II). *Geochim. Cosmochim. Acta* **1999**, *63*, (19-20), 2939-2955.
- 503 35. Hofstetter, T. B.; Heijman, C. G.; Haderlein, S. B.; Holliger, C.; Schwarzenbach, R.
504 P., Complete reduction of TNT and other (poly) nitroaromatic compounds under
505 iron-reducing subsurface conditions. *Environ. Sci. Technol.* **1999**, *33*, (9), 1479-1487.
- 506 36. Jones, A. M.; Kinsela, A. S.; Collins, R. N.; Waite, T. D., The reduction of 4-
507 chloronitrobenzene by Fe (II)-Fe (III) oxide systems-correlations with reduction
508 potential and inhibition by silicate. *J. Hazard. Mater.* **2016**, *320*, 143-149.

- 509 37. Vindedahl, A. M.; Strehlau, J. H.; Arnold, W. A.; Penn, R. L., Organic matter and
510 iron oxide nanoparticles: aggregation, interactions, and reactivity. *Environmental*
511 *Science: Nano* **2016**, *3*, (3), 494-505.
- 512 38. Vindedahl, A. M.; Stemig, M. S.; Arnold, W. A.; Penn, R. L., Character of humic
513 substances as a predictor for goethite nanoparticle reactivity and aggregation. *Environ.*
514 *Sci. Technol.* **2016**, *50*, (3), 1200-1208.
- 515 39. Strehlau, J. H.; Stemig, M. S.; Penn, R. L.; Arnold, W. A., Facet-dependent oxidative
516 goethite growth as a function of aqueous solution conditions. *Environ. Sci. Technol.*
517 **2016**, *50*, (19), 10406-10412.
- 518 40. Huang, J.; Wang, Q.; Wang, Z.; Zhang, H., Interactions and reductive reactivity in
519 ternary mixtures of Fe (II), goethite, and phthalic acid based on a combined
520 experimental and modeling approach. *Langmuir* **2019**, *35*, (25), 8220-8227.
- 521 41. Huang, J.; Dai, Y.; Liu, C.-C.; Zhang, H., Effects of Second Metal Oxides on Surface-
522 Mediated Reduction of Contaminants by Fe (II) with Iron Oxide. *ACS Earth and*
523 *Space Chemistry* **2019**, *3*, (5), 680-687.
- 524 42. Felmy, A. R.; Moore, D. A.; Rosso, K. M.; Qafoku, O.; Rai, D.; Buck, E. C.; Ilton,
525 E. S., Heterogeneous reduction of PuO₂ with Fe (II): Importance of the Fe (III)
526 reaction product. *Environ. Sci. Technol.* **2011**, *45*, (9), 3952-3958.
- 527 43. Felmy, A. R.; Ilton, E. S.; Rosso, K. M.; Zachara, J. M., Interfacial reactivity of
528 radionuclides: emerging paradigms from molecular-level observations. *Mineralogical*
529 *Magazine* **2011**, *75*, (4), 2379-2391.
- 530 44. Schwertmann, U.; Carlson, L.; Fechter, H., Iron oxide formation in artificial ground
531 waters. *Aquatic Sciences-Research Across Boundaries* **1984**, *46*, (2), 185-191.
- 532 45. Larese-Casanova, P.; Kappler, A.; Haderlein, S. B., Heterogeneous Oxidation of
533 Fe(II) on Iron Oxides in Aqueous Systems: Identification and Controls of Fe(III)
534 Product Formation. *Geochimica et Cosmochimica Acta* **2012**, *91*, 171-186.
- 535 46. Jones, A. M.; Griffin, P. J.; Collins, R. N.; Waite, T. D., Ferrous iron oxidation under
536 acidic conditions-The effect of ferric oxide surfaces. *Geochimica et Cosmochimica*
537 *Acta* **2014**, *145*, 1-12.
- 538 47. Colón, D.; Weber, E. J.; Anderson, J. L., QSAR study of the reduction of
539 nitroaromatics by Fe (II) species. *Environ. Sci. Technol.* **2006**, *40*, (16), 4976-4982.
- 540 48. Hartenbach, A. E.; Hofstetter, T. B.; Aeschbacher, M.; Sander, M.; Kim, D.;
541 Strathmann, T. J.; Arnold, W. A.; Cramer, C. J.; Schwarzenbach, R. P., Variability of
542 nitrogen isotope fractionation during the reduction of nitroaromatic compounds with
543 dissolved reductants. *Environ. Sci. Technol.* **2008**, *42*, (22), 8352-8359.

- 544 49. Hartenbach, A.; Hofstetter, T. B.; Berg, M.; Bolotin, J.; Schwarzenbach, R. P., Using
545 nitrogen isotope fractionation to assess abiotic reduction of nitroaromatic compounds.
546 *Environmental science & technology* **2006**, *40*, (24), 7710-7716.
- 547 50. Hofstetter, T. B.; Neumann, A.; Arnold, W. A.; Hartenbach, A. E.; Bolotin, J.;
548 Cramer, C. J.; Schwarzenbach, R. P., Substituent effects on nitrogen isotope
549 fractionation during abiotic reduction of nitroaromatic compounds. *Environmental
550 science & technology* **2008**, *42*, (6), 1997-2003.
- 551 51. Colón, D.; Weber, E. J.; Anderson, J. L., Effect of natural organic matter on the
552 reduction of nitroaromatics by Fe (II) species. *Environmental science & technology*
553 **2008**, *42*, (17), 6538-6543.
- 554 52. Luan, F.; Xie, L.; Li, J.; Zhou, Q., Abiotic reduction of nitroaromatic compounds by
555 Fe(II) associated with iron oxides and humic acid. *Chemosphere* **2013**, *91*, (7), 1035-
556 1041.
- 557 53. Huang, J.; Cao, J.; Tu, N.; Dong, H.; Li, J.; Shou, J.; Li, Y., Effect of surfactants on
558 the removal of nitrobenzene by Fe-bearing montmorillonite/Fe (II). *Journal of colloid
559 and interface science* **2019**, *533*, 409-415.
- 560 54. Cao, J.; Huang, J.; Dong, H.; Li, J.; Shou, J.; Li, Y., Effects of surfactants on the
561 removal of nitrobenzene by Fe (II) sorbed on goethite. *J. Colloid Interface Sci.* **2019**,
562 *552*, 764-770.
- 563 55. King, D. W., Role of carbonate speciation on the oxidation rate of Fe (II) in aquatic
564 systems. *Environmental Science & Technology* **1998**, *32*, (19), 2997-3003.
- 565 56. Gorski, C. A.; Klüpfel, L.; Voegelin, A.; Sander, M.; Hofstetter, T. B., Redox
566 properties of structural Fe in clay minerals. 2. Electrochemical and spectroscopic
567 characterization of electron transfer irreversibility in ferruginous smectite, SWa-1.
568 *Environ. Sci. Technol.* **2012**, *46*, (17), 9369-9377.
- 569 57. Schwertmann, U.; Cornell, R. M., *Iron oxides in the laboratory: preparation and
570 characterization*. John Wiley & Sons: 2008.
- 571 58. Brunauer, S.; Emmett, P. H.; Teller, E., Adsorption of gases in multimolecular layers.
572 *Journal of the American chemical society* **1938**, *60*, (2), 309-319.
- 573 59. Jiang, C. Z.; Tosca, N. J., Fe (II)-carbonate precipitation kinetics and the chemistry of
574 anoxic ferruginous seawater. *Earth. Planet. Sci. Lett.* **2019**, *506*, 231-242.
- 575 60. Tamura, H.; Goto, K.; Yotsuyanagi, T.; Nagayama, M., Spectrophotometric
576 determination of iron (II) with 1, 10-phenanthroline in the presence of large amounts
577 of iron (III). *Talanta* **1974**, *21*, (4), 314-318.

- 578 61. Koppel, D. E., Analysis of macromolecular polydispersity in intensity correlation
579 spectroscopy: the method of cumulants. *The Journal of Chemical Physics* **1972**, *57*,
580 (11), 4814-4820.
- 581 62. Malvern Instruments Ltd, M., Mastersizer 3000 User Manual. **2015**.
- 582 63. Gorski, C. A.; Nurmi, J. T.; Tratnyek, P. G.; Hofstetter, T. B.; Scherer, M. M., Redox
583 behavior of magnetite: Implications for contaminant reduction. *Environmental*
584 *Science & Technology* **2009**, *44*, (1), 55-60.
- 585 64. Huang, J.; Wang, Q.; Wang, Z.; Zhang, H. J., Interactions and Reductive Reactivity
586 in Ternary Mixtures of Fe (II), Goethite, and Phthalic Acid based on a Combined
587 Experimental and Modeling Approach. *Langmuir* **2019**.
- 588 65. Villalobos, M.; Leckie, J. O., Surface complexation modeling and FTIR study of
589 carbonate adsorption to goethite. *Journal of Colloid and Interface Science* **2001**, *235*,
590 (1), 15-32.
- 591 66. van Geen, A.; Robertson, A. P.; Leckie, J. O., Complexation of carbonate species at
592 the goethite surface: Implications for adsorption of metal ions in natural waters.
593 *Geochimica et Cosmochimica Acta* **1994**, *58*, (9), 2073-2086.
- 594 67. Sander, M.; Hofstetter, T. B.; Gorski, C. A., Electrochemical analyses of redox-active
595 iron minerals: a review of nonmediated and mediated approaches. *Environ. Sci.*
596 *Technol.* **2015**, *49*, (10), 5862-5878.
- 597 68. Gorski, C. A.; Aeschbacher, M.; Soltermann, D.; Voegelin, A.; Baeyens, B.; Marques
598 Fernandes, M.; Hofstetter, T. B.; Sander, M., Redox properties of structural Fe in
599 clay minerals. 1. Electrochemical quantification of electron-donating and-accepting
600 capacities of smectites. *Environmental science & technology* **2012**, *46*, (17), 9360-9368.
- 601 69. Arnold, W. A.; Roberts, A. L., Pathways and kinetics of chlorinated ethylene and
602 chlorinated acetylene reaction with Fe (0) particles. *Environ. Sci. Technol.* **2000**, *34*,
603 (9), 1794-1805.
- 604 70. Scherer, M. M.; Balko, B. A.; Gallagher, D. A.; Tratnyek, P. G., Correlation analysis
605 of rate constants for dechlorination by zero-valent iron. *Environmental science &*
606 *technology* **1998**, *32*, (19), 3026-3033.
- 607 71. Villalobos, M.; Trotz, M. A.; Leckie, J. O., Surface complexation modeling of
608 carbonate effects on the adsorption of Cr (VI), Pb (II), and U (VI) on goethite.
609 *Environmental science & technology* **2001**, *35*, (19), 3849-3856.
- 610 72. Villalobos, M.; Leckie, J. O., Carbonate adsorption on goethite under closed and
611 open CO₂ conditions. *Geochimica et Cosmochimica Acta* **2000**, *64*, (22), 3787-3802.
- 612 73. White, A. F.; Peterson, M. L., Role of reactive-surface-area characterization in
613 geochemical kinetic models. In ACS Publications: 1990.

- 614 74. Liu, J.; Aruguete, D. M.; Murayama, M.; Hochella Jr, M. F., Influence of size and
615 aggregation on the reactivity of an environmentally and industrially relevant
616 nanomaterial (PbS). *Environmental science & technology* **2009**, *43*, (21), 8178-8183.
- 617 75. Cornell, R. M.; Schwertmann, U., *The iron oxides: structure, properties, reactions,*
618 *occurrences and uses.* John Wiley & Sons: 2003.
- 619 76. Baalousha, M., Aggregation and disaggregation of iron oxide nanoparticles: influence
620 of particle concentration, pH and natural organic matter. *Science of the total*
621 *Environment* **2009**, *407*, (6), 2093-2101.
- 622 77. Daugherty, E. E.; Gilbert, B.; Nico, P. S.; Borch, T., Complexation and Redox
623 Buffering of Iron(II) by Dissolved Organic Matter. *Environmental Science &*
624 *Technology* **2017**, *51*, (19), 11096-11104.
- 625 78. Rose, A. L.; Waite, T. D., Kinetics of iron complexation by dissolved natural organic
626 matter in coastal waters. *Marine chemistry* **2003**, *84*, (1), 85-103.
- 627